PAPER

Cryogenic characteristics of GaAs-based near-infrared light emitting diodes

To cite this article: Peng Bai *et al* 2020 *Semicond. Sci. Technol.* **35** 035021

View the article online for updates and enhancements.

IOP **ebooks**™

Bringing together innovative digital publishing with leading authors from the global scientific community.

Start exploring the collection−download the first chapter of every title for free.

Cryogenic characteristics of GaAs-based near-infrared light emitting diodes

Peng Bai[1,4] ⓘ, Yueheng Zhang[1,4,6], Tianmeng Wang[1,5], Zhiwen Shi[1,4], Xueqi Bai[1], Chaoying Zhou[1], Yaning Xie[1], Lujie Du[1], Mengting Pu[1], Zhanglong Fu[2], Juncheng Cao[2], Xuguang Guo[3] and Wenzhong Shen[1,4]

[1] Key Laboratory of Artificial Structures and Quantum Control, School of Physics and Astronomy, Shanghai Jiao Tong University, Shanghai 200240, People's Republic of China
[2] Key Laboratory of Terahertz Solid-State Technology, Shanghai Institute of Microsystem and Information Technology, Chinese Academy of Sciences, Shanghai 200050, People's Republic of China
[3] School of Optical-Electrical and Computer Engineering, University of Shanghai for Science and Technology, Shanghai 200093, People's Republic of China
[4] Collaborative Innovation Center of Advanced Microstructures, Nanjing, 210093, People's Republic of China
[5] Department of Chemical and Biological Engineering, Rensselaer Polytechnic Institute, Troy, NY 12180, United States of America

E-mail: yuehzhang@sjtu.edu.cn

Abstract

High performance infrared light emitting diodes (LEDs) have drawn wide attention because of their significant applications in biomedicine, agriculture, aquaculture, night vision security systems and scientific researches. Due to the rapid development of infrared up-conversion devices, especially in the terahertz region, the studies on the GaAs-based infrared LEDs operating at low temperature (<20 K) are quite needed. In this paper, two representative GaAs-based LEDs (GaAs/AlGaAs double heterostructure LED (DH-LED) and GaAs (InGaAs)/ AlGaAs quantum well infrared LED (QW-LED)) are fabricated and characterized with electroluminescence (EL) spectroscopy and electroluminescence efficiency (ELE) at different temperatures. The ELE of the QW-LED is about 70% higher at low temperatures (<150 K) but lower at high temperatures (>150 K) than that of the DH-LED. A developed rate equation method is used to analyze the ELE superiority of the QW-LED. Finally, the surface EL uniformity of the two LEDs is studied by using the charge coupled devices imaging. This study provides a guidance to choose and design LED structures for different operation temperatures.

1. Introduction

Light emitting diodes (LEDs), unlike conventional light sources, generate high light level with less heat, compact structure, low-cost and save on electricity. After nearly one century development, the LEDs have been widely used in optical-fiber-based communication, medical services, status indicator lamps, LED displays and general illumination [1–3]. For the applications in the range from the ultraviolet to the near-infrared, where there needs the light, there is the LED.

As the oldest LED device, the infrared LED plays an important role in the applications of biomedicine fields, agriculture, aquaculture, night vision security systems and scientific researches [4]. In addition, infrared LED has been extensively used in the semiconductor up-conversion technology which is driven by the potential application of pixelless imaging and single photon detection [5–10].

The semiconductor up-conversion technology relies on the epitaxial growth integration of a photodetector and a LED. The two devices are serially connected. With two decades of development, the pixelless imaging devices based on the semiconductor up-conversion technique have made tremendous

---

[6] Author to whom any correspondence should be addressed.

progress at near-infrared [7, 8], mid-infrared [5, 6], as well as terahertz region [10]. This imaging scheme simplifies the device fabrication process significantly and reduces the cost greatly. Beyond that, it solves the mismatch problem between the readout integrated circuit with array detection pixels in many situations [10, 11]. In addition to the pixelless imaging, the semiconductor up-conversion technique has also been proposed for a novel idea of single photon detector [9]. It provides a new single photon detection scheme for telecom band and attracts much attention. Recently, the up-conversion technique has been extended to the terahertz (THz) region [10]. Unlike the near-infrared or mid-infrared application, the THz up-conversion devices usually work at lower temperatures (<20 K).

As the essential part of the semiconductor up-conversion device, the performances of the LED directly determine the up-conversion efficiency and therefore affect the imaging quality and single photon detection efficiency. GaAs-based infrared LEDs have been widely used in various infrared up-conversion devices. The two most commonly used LED structures in the infrared up-conversion devices are GaAs/AlGaAs double heterostructure LED (DH-LED) and GaAs(InGaAs)/AlGaAs quantum well infrared LED (QW-LED). The DH-LED has been systematically investigated and optimized for the room temperature and liquid nitrogen temperature operation [12, 13]. The only difference of the QW-LED is that there is an $In_{0.1}Ga_{0.9}As$ quantum well in the center of the GaAs active region. The greatest advantage of this structure is that the reabsorption of the emitted photons could be restricted greatly, which is good to the imaging quality [14].

In light of the important application in the THz upconverter, with the continuous development of technology, infrared LEDs are increasingly possible to be used under the cryogentic temperatures. Other potential cryogenic application, e.g. electroluminescence cooling and quantum computing [15–18], call for the investigation on the performance of infrared LED at low temperatures either. Imangholi *et al* investigated the photoluminescence properties in GaAs/GaInP heterojunction structure from 7 K–300 K [19]. However, there is few systematic investigation on the cryogenic characteristic of the present two types of LED. The lowest temperature for such two types of LED in previous study is just as low as 65 K [13]. What is the performance of these LEDs at cryogenic temperatures and how to choose or design proper LED at such low temperatures are still open questions. Therefore, it is necessary and meaningful to carry out an investigation for the LED working in low temperatures.

In this work, we systematically investigate the temperature dependent properties of the two typical GaAs-based LEDs, which were widely used in the infrared up-conversion technology. Both the DH-LED and QW-LED are fabricated. Temperature dependent electroluminescence spectrum and efficiency are measured and compared from 4 K to room temperature. The reason of high electroluminescence efficiency of QW-LED at low temperature is discussed. The detailed recombination mechanism at different temperatures of the QW-LED is studied using a developed rate equation analytical model. Finally, the electroluminescence hotspots at

low temperatures with low injection level are also studied and discussed.

2. Device structure

The device structures of the DH-LED and QW-LED are shown in figures 1(a) and (b). The p-GaAs active region is sandwiched by a pair of $Al_xGa_{1-x}As$. The major difference between the two LEDs is that there is a 9 nm $In_{0.1}Ga_{0.9}As$ quantum well at the center of the active region of the GaAs QW-LED. The Al (In) composition distribution and the band diagram of DH-LED and QW-LED are shown in figures 1(c) and (d) respectively. Both of the LED structures adopted the graded hetero-interfaces between the active layer and the barrier layer, which caused the minor band offset at the interfaces. The Al component grading layer and the grading doping concentration is aim to improve the current injection efficiency and the carrier confinement efficiency. On the one hand, barriers caused resistance at the heterointerfaces could be effectively reduced or completely eliminated by Al composition grading layer just shown in the band diagram in figures 1(c), (d) [20]. On the other hand, the thermal power produced by the interface resistances leads to heating of the active region would be reduced, thereby increasing the radiative recombination efficiency.

Both of the DH-LED and QW-LED were grown on the Si-doped GaAs(100) substrate to realize high material quality. The wafer growth started with a lattice matched 250 nm $Al_{0.45}Ga_{0.55}As$ blocking layer followed by 50 nm buffer layer. Then the wafer growth continued with the LED layers. The doping concentration in GaAs area of the active region are 7×10^{17} cm^{-3} and 1×10^{17} cm^{-3} for the DH-LED and QW-LED respectively. The minor thickness difference of the active region (400 nm for DH-LED and 399 nm for QW-LED) has no influence on the luminescence, considering the total thickness of the active region. Detailed LED structures of the DH-LED and QW-LED were shown in table 1.

The samples were processed using standard photolithographic techniques. Square mesas of various sizes (400×400 μm^2, 600×600 μm^2 and 1000×1000 μm^2) were patterned and dry etched. After mesa etching, the top ring p-contact metals Ti/Pt/Au and bottom n-contact metals PdGe/Ti/Pt/Au were deposited separately using the standard lift-off process. The devices were mounted on 14 pin packages for electrical and optical measurements. The measurements were carried out in a cryostat at different temperatures. The emission spectrum of LED was measured using a fiber spectrometer (Ocean optics QE65PRO). The optical fiber probe was close to the glass window of the cryostat to acquire the emission spectrum. The external quantum efficiency of LED was calculated from the driving current and emission light power. The emission light power was measured with Thorlabs S130C large area Si slim photodiode placed close enough to the LED. At low temperatures, the emission power had to be measured with Thorlabs S130C outside of the cryostat. The actual emission power should compensate with a calibration coefficient, which is the emission power ratio when LED is put outside and inside of the cryostat.
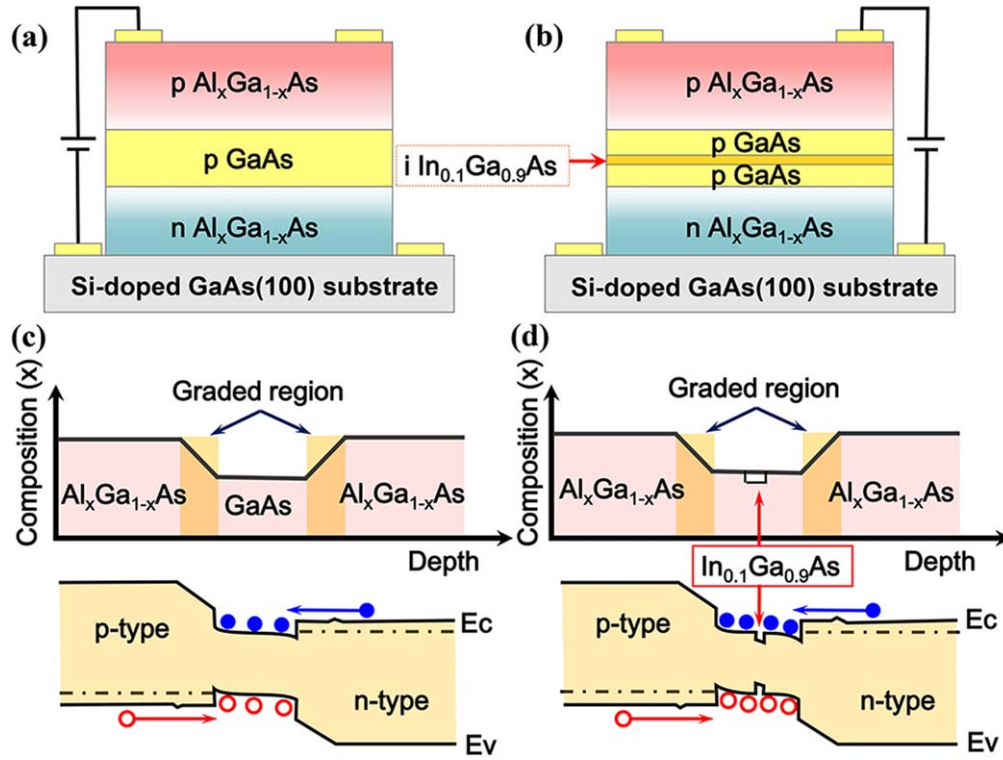
Figure 1. (a) Device structure of the DH-LED. (b) Device structure of the QW-LED. (c) Composition distribution and the band diagram of GaAs/AlGaAs double heterostructure LED. (d) Composition distribution and the band diagram of GaAs (InGaAs)/AlGaAs quantum well LED.

Table 1. The detailed wafer structures of the DH-LED and QW-LED. The structure difference of the two LEDs is the active layer (seventh layer). The active layer of DH-LED is 400 nm GaAs and p-doped with Be acceptor. For the QW-LED, there is a 9 nm $In_{0.1}Ga_{0.9}As$ quantum well at the center of the active region.

Layer ID	Material	Composition	Thickness(Å)	Dopant	Doping type	Concentration(cm^{-3})
12	GaAs	—	500	Be	p	2.00E + 19
11	AlxGa1-xAs	x = 0.10	3500	Be	p	2.00E + 19
10	AlxGa1-xAs	x = 0.30 => 0.10	500	Be	p	2.00E + 19
9	AlxGa1-xAs	x = 0.30	1000	Be	p	2.00E + 18 => 2.00E19
8	AlxGa1-xAs	x = 0.15 => 0.30	400	—	—	—
7(DH-LED)	GaAs	—	4000	Be	p	7.00E + 17
7(QW-LED)	GaAs	—	1950	Be	p	1.00E + 17
7(QW-LED)	InyGa1-yAs	y = 0.10	90	—	—	—
7(QW-LED)	GaAs	—	1950	Be	p	1.00E + 17
6	AlxGa1-xAs	x = 0.30 => 0.15	400	—	—	—
5	AlxGa1-xAs	x = 0.30	1000	Si	n	1.00E + 18
4	AlxGa1-xAs	x = 0.10 => 0.30	500	Si	n	2.50E + 18
3	AlxGa1-xAs	x = 0.10	3500	Si	n	2.50E + 18
2	GaAs	—	500	Si	n	2.50E + 18
1	AlxGa1-xAs	x = 0.45	2500	Si	n	2.50E + 18
			Si-doped GaAs(100) substrate			

3. Electroluminescence (EL) spectrum

The temperature dependent electroluminescence spectra of the DH-LED and QW-LED were displayed in figures 2(a) and (b) respectively. To make the data strictly comparable, the emission spectra at different applied current and temperatures were measured with the same integral time. Figure 2(a) shows only one electroluminescence peak for the DH-LED at all measured

temperatures. It originates from the radiation recombination of the GaAs active region. As the temperature increases, the peak positon of the EL spectrum shows an evident redshift because of the energy gap decreases due to the Varshni effect.

In contrast to the DH- LED, the QW-LED shows different EL spectra. The main EL peak shows red-shift from 870 nm to 930 nm from 4 K to room temperature either. It is clear that at the temperatures below 100 K the dominant luminescence peaks
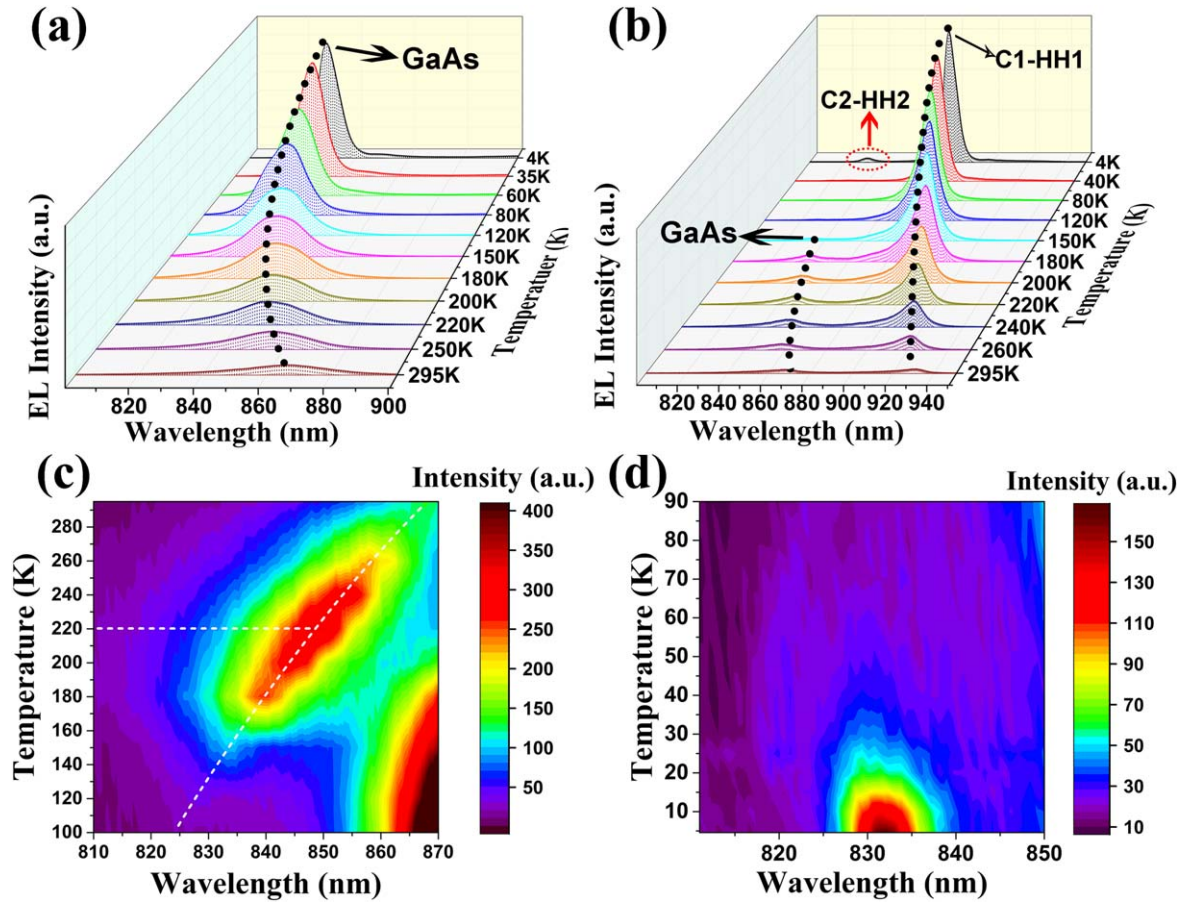
Figure 2. (a) Temperature dependent EL spectra of the DH-LED with 1 mA driving current. (b) Temperature dependent EL spectra of the QW-LED with 1 mA driving current. (c) Mapping result of the EL intensity of QW-LED as a function of temperatures (100–295 K) and wavelength (810–870 nm) with 1 mA driving current. (d) Mapping result of the EL intensity of QW-LED as a function of temperatures (4–90 K) and wavelength (810–850 nm) with 1 mA driving current.

of QW-LED indeed differ by 60 nm compare with DH-LED. This is resulted from the structure difference of such two LEDs, i.e. there is an 9 nm $In_{0.1}Ga_{0.9}As$ quantum well in the QW-LED. When the temperature falls in the range of 100–295 K, an extra EL peak appears and shifts from 830 nm to 870 nm and the corresponding EL intensity increases first and then decreases (presented in figure 2(c)). As the temperature goes down to 50 K, another small EL peak around 833 nm occurs, as shown in figures 2(b) and (d).

To better understand the origin of the QW-LED electroluminescence, the band structure of the $In_{0.1}Ga_{0.9}As$/GaAs quantum well was calculated by self-consistent solving the Schrodinger equation [21, 22]. The plane wave expansion method was used for accurate calculation and the lattice mismatch caused strain and bias caused Stark shift were neglected. The band-gaps of GaAs and $In_{0.1}Ga_{0.9}As$ are taken as 1.518959 eV and 1.36495 eV at 4 K respectively [10]. The ratio of conduction and valence band offsets is set as 6:4. The effective masses of the well (m_w^*) and barrier (m_b^*) are ($m_w^* = 0.05873m_0$, $m_b^* = 0.063m_0$) for electron, ($m_w^* = 0.5m_0$, $m_b^* = 0.51m_0$) for heavy hole respectively with m_0 the electron mass[7]. The self-consistent

solutions of the calculation agree well with experiment results. The main EL peaks existing at all temperatures are related to the first conduction-subband to the first heavy hole subband transition ($C1 \rightarrow HH1$) of the InGaAs quantum well, corresponding to the calculated transition energy of 1.3999 eV (885.7 nm). The peaks existing only in the range of 100–295 K are from the spontaneous recombination of the GaAs barrier. The peak at 833 nm below 50 K originates from the second conduction-subband to the second heavy hole subband transition ($C2 \rightarrow HH2$) of the InGaAs quantum well (the calculated transition energy is 1.4807 eV (837.4 nm)). As the temperature increases from 4 K to 50 K, the intensity of the main EL peak from the $C1 \rightarrow HH1$ transition remains almost unchanged. However, the $C2 \rightarrow HH2$ transition induced luminescence peak gradually fade away. We attribute this to the decrease of the radiation recombination rate because of the carrier loss caused by the thermal excitation. It should be noted that there is only luminescence from InGaAs quantum well below 100 K. No detectable light emitting signal from GaAs is observed. This is because low doping concentration and low effective ionization rate in GaAs, leading to low carrier concentration and thereby low radiative recombination. From 50 K to 100 K, the luminescence is dominated by $C1 \rightarrow HH1$ transition in the $In_{0.1}Ga_{0.9}As$
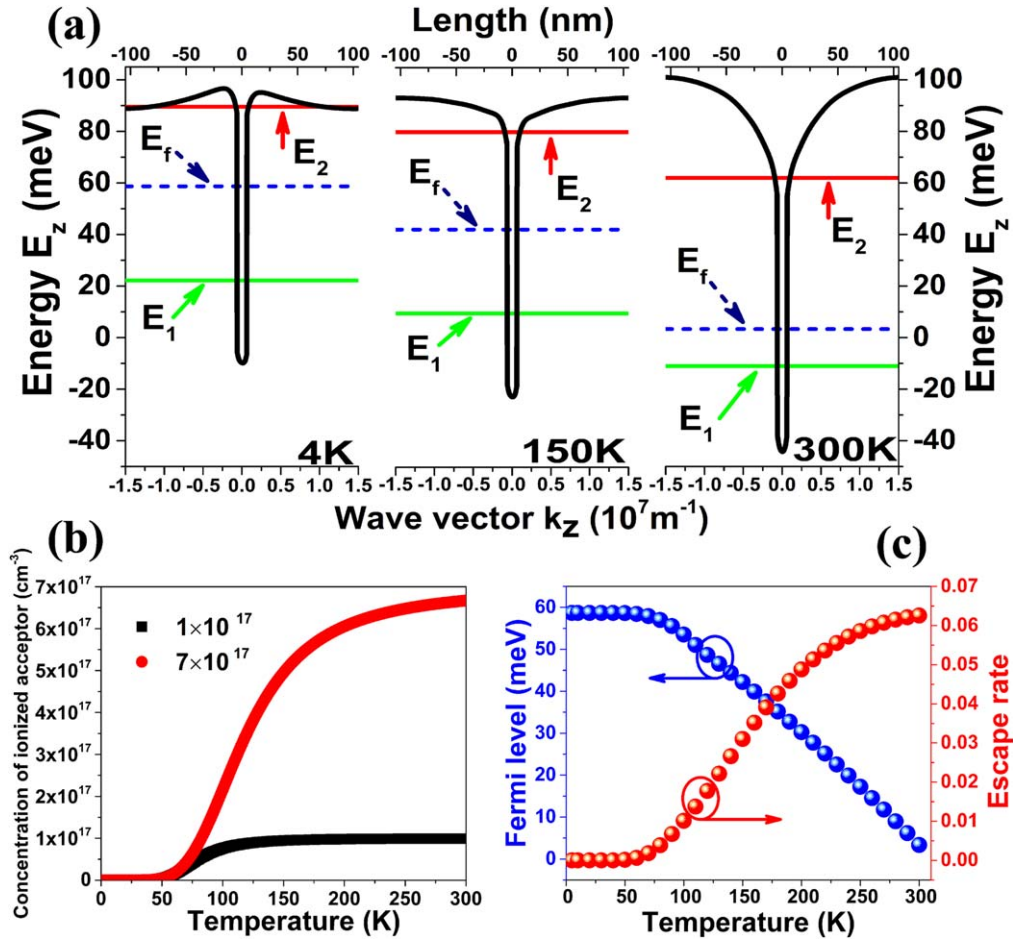
Figure 3. (a) Calculated band structures of the quantum well in QW-LED at 4 K, 150 K and 300 K. The dashed lines are the Fermi levels. (b) Temperature dependent concentration of the ionized acceptor in the active area of the two LEDs (DH-LED with 7×10^{17} cm^{-3} and QW-LED with 1×10^{17} cm^{-3}). (c) Calculated temperature dependent Fermi level and escape rate.

quantum well. When temperature is higher than 100 K, the spontaneous recombination peak of the GaAs appears because of two possible reasons. Firstly, as shown in figure 3(b), the doping acceptors (Be) are well ionized at this high temperature, which are calculated using the partial ionization theory of the acceptors in semiconductor [23]. Secondly, the effect of carrier confinement for the quantum well is greatly reduced at such 'high' temperatures. Figure 3(a) shows the calculated band structures of the quantum well in QW-LED at 4 K, 150 K and 300 K with a same electron injection level. The reference point (zero energy) for E_n is chosen at the conduction bandedge of the well without taking the manybody effect into consideration. We can find that the barrier confinement effect vanishes and the fermi level reduces with the temperature increasing. The temperature dependent fermi levels are presented in figure 3(d). The fermi level droops significantly when the temperature is higher than 100 K. Meanwhile, the escape rate (defined as $R_{escape} = \exp(-(E_B - E_F)/kT)$ [24], where E_B is the barrier energy of the quantum well, E_F is the fermi level, k is the Boltzmann constant and T is temperature.) of the electron in quantum well increases obviously. Such collective effect from the carrier varation in the GaAs active layer and the InGaAs quantum well explain the relative changes of EL peaks from 100 K to room temperature.

4. Temperature dependent EL efficiency

The electroluminescence efficiency (ELE) was used to evaluate the performance of the LED, which is defined as output EL power divided by driving current and is proportional to the EL external quantum efficiency. The mapping results of the ELE as a function of driving current density and temperature for the two LEDs were presented in the figure 4(a) (QW-LED) and figure 4(b) (DH-LED) respectively. Because of the the total reflection at the air/semiconductor interface, the direct photon escape probability is only 1.33%, corresponding to the ELE is 0.0189 W A^{-1}. Thanks to the photon recycing effect, the peak ELE for the two LEDs could reach as high as 0.05 W A^{-1} (QW-LED) and 0.025 W A^{-1} (DH-LED) respectively.

The figures reveal that the two LEDs show an evident efficiency droop with the temperature increasing from 4 K to room temperature at any driving current density. At a certain temperature, the ELE increases first and then decreases with the driving current density increasing. The injection current dependent efficiency droop is a common phenomenon in LED [25], which is mainly caused by the increase of the non-radiative recombination. The efficiency peak point shifts to higher current densities as temperature increases because the
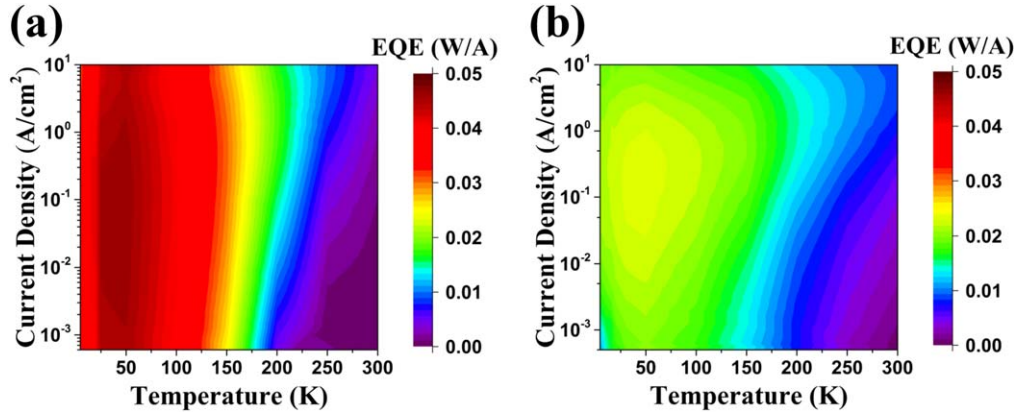
Figure 4. (a) Mapping result of the ELE for QW-LED as a function of temperatures and injection current densities. (b) Mapping result of the ELE for DH-LED as a function of temperatures and injection current densities.

Shockley–Reed–Hall (SRH) recombination increases with temperature increasing. It should be noted that at low temperatures (<200 K), the efficiency of the QW-LED is higher than that of the DH-LED. But at the high temperature (>200 K), the result is opposite. This change is particularly evident in figures 5(g)–(i).

The ELE comparisons of the two LEDs at the temperatures of 4 K, 50 K, 100 K, 150 K, 200 K and 250 K are presented in figures 5(a)–(f). It is obvious that the ELE of the QW-LED is higher than that of the DH-LED when temperature is lower than 200 K. At 200 K, the ELE of the DH-LED exceeds that of the QW-LED at low injection current density (as shown in figure 4(e)). As the temperature continue to rise, the ELE of the DH-LED becomes higher than that of QW-LED at all current densities gradually. The comparison results also reveal that the current density dependent efficiency droop is more evident at high temperatures, which is due to the relative high nonradiative recombination probability at high temperatures. The temperature dependent ELE comparisons of the two LEDs at the driving current of $0.0125 \, \mathrm{A \, cm^{-2}}$, $0.125 \, \mathrm{A \, cm^{-2}}$ and $1.25 \, \mathrm{A \, cm^{-2}}$ were shown in figures 5(g)–(i). With three different driving current densities, the results show the same trends. If the temperature was higher than about 200 K, the ELE of the DH-LED will be higher than QW-LED. When the operation temperature is lower than about 200 K, the performance of the QW-LED is much better than DH-LED. This result provides us a guidance to choose the LED for different operation temperatures. The temperature dependent difference between the two LEDs will be discussed in detail below.

To better understand the superiority of the QW-LED at low temperatures and the severe efficiency droop at high temperatures, we should make clear the recombination mechanism at different temperatures. The non-radiative SRH recombination, radiative recombination, and Auger recombination together determine the luminescence property of the LED. The ABC model is a simple and widely used approach to study these three principal channels of recombination in LED [26, 27]. The temperature dependent recombination mechanism of the LED will be much clearer if the SRH (A), radiative (B), and Auger recombination (C) coefficients at all

temperatures were given. Thus the most direct way to study the LED performance is to measure the three coefficients at different temperatures. However, it is impractical and difficult to realize the measurement at such an extreme low temperature directly (∼4 K).

A developed ABC model by Ryu *et al* provides an alternative way to analyze the LED performance with a single fit parameter, the maximum internal quantum efficiency [28]. The advantage of this method is that the internal quantum efficiency and each recombination current at arbitrary current density and temperatures can be unambiguously determined without any knowledge of A, B, and C coefficients. The internal quantum efficiency (*IQE*) η_i depends on the injection current explicitly by numerically solving the equation:

$$\eta_i = 1 - \frac{(1 - \eta_{max})}{2J}\left(1 + \frac{\eta_i J}{\eta_{max} J_{max}}\right)\sqrt{\frac{\eta_i J J_{max}}{\eta_{max}}} \quad (1)$$

where η_i is the internal quantum efficiency, J is the injection current density and η_{max} and J_{max} are the maximum value of IQE and the corresponding injection current density. J_{max} is exactly known by the measurement of the current density dependent ELE and η_{max} can be fitted in terms of the measurement results. This method points out that there exists only one IQE curve for given J_{max} and η_{max} regardless of A, B, and C coefficients.

The fitted J_{max} and η_{max} at different temperatures are displayed in figure 6. Moreover, each recombination current density can be deduced if the J_{max} and η_{max} were given:

$$J_{SRH} = \frac{1 - \eta_{max}}{2}\sqrt{\frac{\eta_i J J_{max}}{\eta_{max}}},$$

$$J_{Rad} = \eta_i J, \quad J_{Auger} = \frac{\eta_i J(1 - \eta_{max})}{2\eta_{max}J_{max}}\sqrt{\frac{\eta_i J J_{max}}{\eta_{max}}}. \quad (2)$$

Using equation (2), the recombination current distribution at any temperatures can be fitted and analyzed.

The fitted recombination current density distribution of QW-LED and DH-LED at different temperatures with the injection current level of $0.0125 \, \mathrm{A \, cm^{-2}}$, $0.125 \, \mathrm{A \, cm^{-2}}$ and $1.25 \, \mathrm{A \, cm^{-2}}$ were presented in figures 7(a)–(f). Due to the relative low injection level, the Auger recombination in the
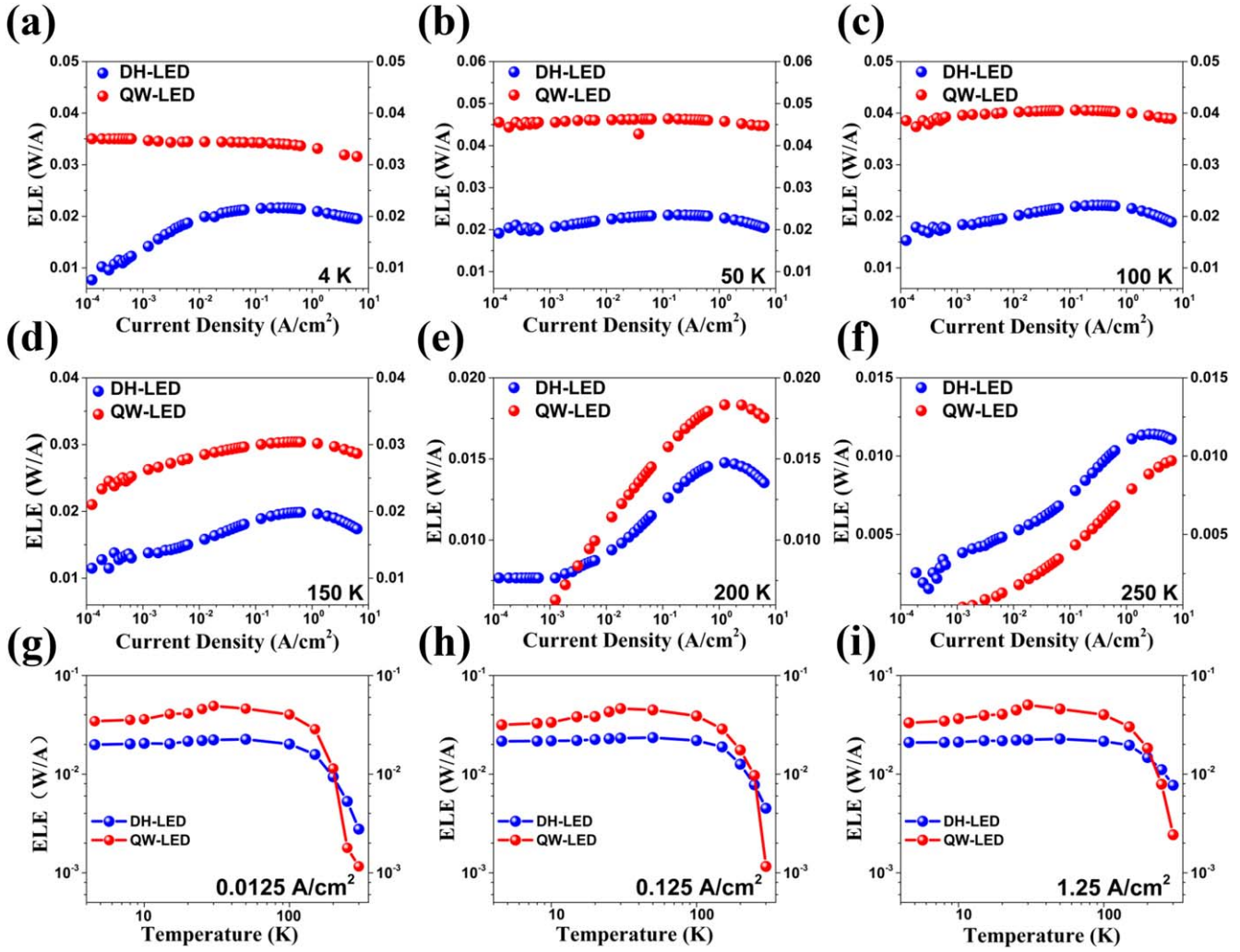
Figure 5. The driving current density dependent ELE comparisons of the two LEDs at the temperatures of (a) 4 K, (b) 50 K, (c) 100 K, (d) 150 K, (e) 200 K and (f) 250 K. The temperature dependent ELE comparisons of the two LEDs at the driving current of (g) 0.0125 A cm^{-2}, (h) 0.125 A cm^{-2} and (i) 1.25 A cm^{-2}.
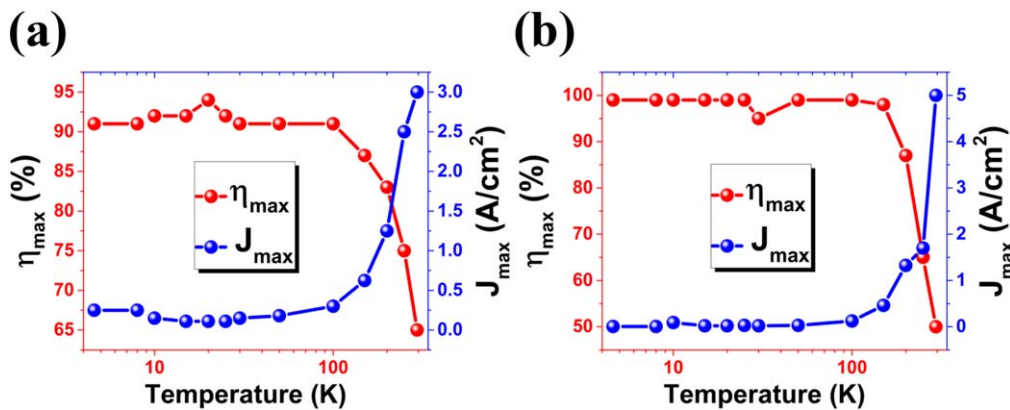

Figure 6. (a) Temperature dependent η_{max} and J$_{max}$ of DH-LED. (b) Temperature dependent η_{max} and J$_{max}$ of QW-LED.

QW-LED is extreme low at nearly all temperatures. Therefore, the luminescence of the QW-LED is determined by the radiative recombination and the SRH recombination. It is obvious that the radiative recombination dominates the luminescence when the temperature is lower than 200 K.

When the temperature increases, the proportion of the SRH and radiative recombination current changes and the SRH recombination dominates at room temperatures [12]. The balance temperature of the SRH and radiative recombination increases with the increasing of the injection current density.
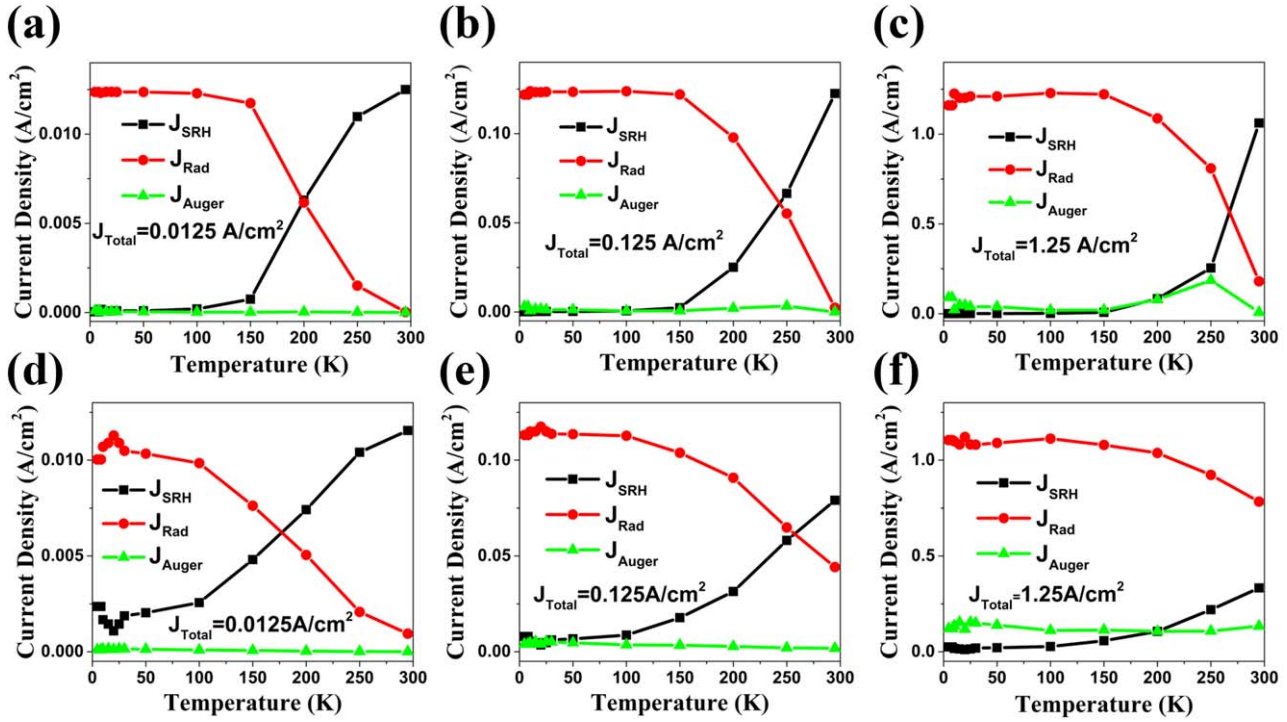
Figure 7. The fitted recombination current density distribution of QW-LED at different temperatures with the injection current level of (a) 0.0125 A cm^{-2}, (b) 0.125 A cm^{-2} and (c) 1.25 A cm^{-2}, respectively. The fitted recombination current density distribution of DH-LED at different temperatures with the injection current level of (d) 0.0125 A cm^{-2}, (e) 0.125 A cm^{-2} and (f) 1.25 A cm^{-2}, respectively.

Additionally, the SRH recombination in the QW-LED is higher than that in DH-LED, especially at high temperatures with large driving current. This could exactly explain the efficiency change in figures 5(g)–(i). The efficiency droop is mainly caused by two reasons. Firstly, the carrier confinement in the quantum well weakened at higher temperatures, which causes the decreases of the radiative recombination rate. Secondly, as shown in figure 7, the SRH recombination rate increases significantly as the temperature increases.

Based on the above analysis, the difference between the two LEDs in the figures 5(a)–(i) is easy to understand. At low temperatures, the carrier confinement is more effective in the In$_{0.1}$Ga$_{0.9}$As quantum well of the QW-LED. Additionally, the emission photon energy of the QW-LED is lower than the band gap of any other material in the QW-LED. Therefore the reabsorption of the emitted photons is greatly reduced in QW-LED. Owing to the higher carrier confinement efficiency and lower photon reabsorption, the ELE of the QW-LED is about 70% higher than that of DH-LED at low temperatures (<150 K). As for high temperatures condition, the luminescence of the QW-LED is resulted from the quantum well luminescence and the GaAs barrier luminescence. The carrier confinement of In$_{0.1}$Ga$_{0.9}$As quantum well goes weak, leading to the relative low luminescence intensity from QW for the same total injection current. Besides, the doping concentration of the GaAs barrier of the QW-LED is lower than that of the DH-LED, which results in lower radiative recombination from GaAs barrier luminescence in contrast to the case of DH-LED [12]. Due to the low injection level and low doping concentration, the ELE of the QW-LED is lower than that of DH-LED at high temperatures (>150 K).

5. Hot spots

The surface EL uniformity for the two LEDs is important when it was used in infrared up-conversion devices, especially imaging devices. The localized bright EL spots called hot spots have been observed in the integrated (QWP-LED) up-conversion devices. Wasilewski *et al* have systematically investigated the hot spots with reliable experiment [29]. The formation mechanism of the hot spots was explained as the low resistance path caused by a local alloy separation in ternary layers, induced by floating organic molecules or molecular contamination clusters caused nanowire-like defects [29]. This could also explain the origin of the hot spots in the single DH-LED and QW-LED studied in this work. The hot spots can be readily observed only at low temperatures (<100 K).

The temperature of previous studies is around liquid nitrogen temperature, which is the operation temperature of the mid-infrared QWPs. If the LED was used in the THz up-conversion devices, the operation temperature will be much lower and even close to liquid helium temperature [22]. Here, we observed and studied the hot spots characteristics at low temperatures (4–80 K) of the DH-LED and QW-LED respectively.

The injection current dependent charge coupled devices (CCD) mapping image of DH-LED, temperature dependent CCD mapping image of DH-LED and QW-LED were displayed in figures 8(a)–(c). The luminescence of the hot spots are extremely evident with low injection level (as shown in figure 8(a)), which is caused by the nanowire defects resulted in the low resistance path below the hot spot. Because the low
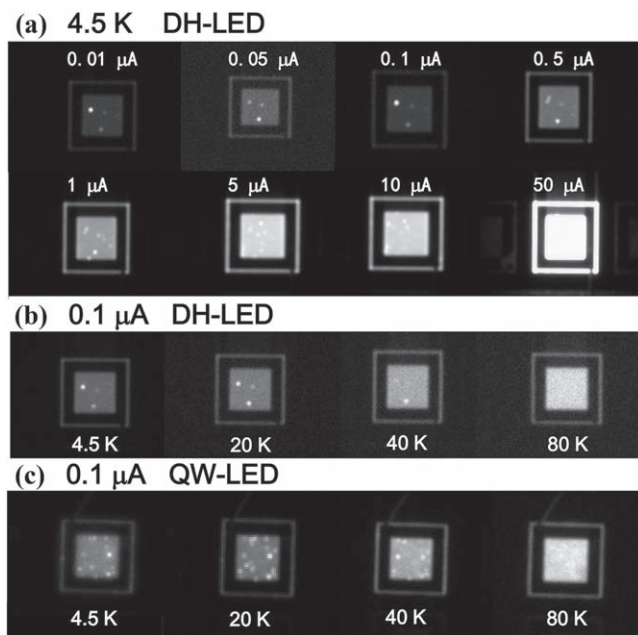
Figure 8. (a) Injection current dependent CCD mapping image of DH-LED. (b) Temperature dependent CCD mapping image of DH-LED. (c) Temperature dependent CCD mapping image of QW-LED.

resistance paths are capable of shunting currents by several orders of magnitude higher than the neighbouring material, the injection carriers first choose the low resistance path to pass the barrier region and then inject to the active layer for recombination.

The luminescence intensity of the uniform background increases with the current increasing. When the driving current increased to $5\,\mu A$ ($3.125 \times 10^{-3}\,A\,cm^{-2}$), the hot spots could not be recognized from the uniform background. For a certain driving current, the luminescence intensity of the uniform background also increases as the temperature increases (as shown in figures 8(b) and (c)), which is due to the increase of the ionization rate of the impurity in the active layer as temperature increases (shown in figure 3(b)). Comparing figures 8(b) and (c), we can find that the hot spots density of QW-LED is about one order of magnitude higher than DH-LED at the same temperature with the same driving current. It could be caused by the extra mismatch between the $In_{0.1}Ga_{0.9}As$ and the GaAs interface, which may lead to more low resistance paths inside the LED devices. Therefore, the issue of the hotspots in the DH-LED should be carefully suppressed as possible by improve the epitaxial growth quality and special settlement should be carried out for large scale up-conversion pixelless imaging [30].

6. Conclusion

In conclusion, we systematically investigated the temperature dependent properties of the two typical GaAs-based LEDs (GaAs/AlGaAs double heterostructure LED (DH-LED) and GaAs(InGaAs)/AlGaAs quantum well infrared LED (QW-LED)). Both the DH-LED and QW-LED were fabricated

and characterized with temperature dependent EL spectroscopy and electroluminescence efficiency (ELE). The DH-LED showed only one EL peak at any temperatures. Instead, the QW-LED showed different EL peaks at different temperatures. The extra EL peaks of the QW-LED at specific temperatures were due to the complexity of the introduced quantum well. The ELE of the QW-LED is about 70% higher than that of the DH-LED at low temperatures ($<150\,K$) but lower than the DH-LED at high temperatures ($>150\,K$). A developed rate equation method was used to analyze the ELE properties of the two LEDs at different temperatures. Finally, the temperature and current dependent surface EL uniformities of the two LEDs were observed and studied by using the charge coupled devices (CCD) imaging.

ORCID iDs

Peng Bai ⓘ https://orcid.org/0000-0001-9541-3489

References

[1] Singh P and Tan C M 2016 A review on the humidity reliability of high power white light LEDs *Microelectron. Reliab.* **61** 129
[2] Chang M H, Das D, Varde P V and Pecht M 2012 Light emitting diodes reliability review *Microelectron. Reliab.* **52** 762
[3] Krames M R, Shchekin O B, Mach R M, Mueller G O, Zhou L, Harbers G and Craford M G 2007 Status and future of high-power light-emitting diodes for solid-state lighting *J. Disp. Technol.* **3** 2
[4] Yeh N, Ding T J and Yeh P 2015 Light-emitting diodes' light qualities and their corresponding scientific applications *Renew. Sustain. Energy Rev.* **51** 55
[5] Allard L B, Liu H C, Buchanan M and Wasilewski Z R 1997 Pixelless infrared imaging utilizing a p-type quantum well infrared photodetector integrated with a light emitting diode *Appl. Phys. Lett.* **70** 2784
[6] Dupont E, Liu H C, Buchanan M, Wasilewski Z R, St-Germain D and Chevrette P 1999 Pixel-less infrared imaging based on the integration of an n-type quantum-well infrared photodetector with a light-emitting diode *Appl. Phys. Lett.* **75** 563
[7] Ban D, Luo H, Liu H C, Wasilewski Z R and Buchanan M 2005 Pixelless 1.5-m up-conversion imaging device fabricated by wafer fusion *IEEE Photonics Technol. Lett.* **17** 7
[8] Chen J, Tao J, Ban D, Helander M G, Wang Z, Qiu J and Lu Z 2012 Hybrid organic/inorganic optical up-converter for pixel-less near-infrared imaging *Adv. Mater.* **24** 3138

[9] Bai P, Zhang Y H and Shen W Z 2017 Infrared single photon detector based on optical up-converter at 1550 nm *Sci. Rep.* **7** 15341

[10] Fu Z L, Gu L L, Guo X G, Tan Z Y, Wan W J, Zhou T, Shao D X, Zhang R and Cao J C 2016 Frequency up-conversion photontype terahertz imager *Sci. Rep.* **6** 25383

[11] Rogalski A and Sizov F 2011 Terahertz detectors and focal plane arrays *Opto-Electron. Rev.* **19** 3

[12] Ban D, Luo H, Liu H C, Wasilewski Z R, SpringThorpe A J, Glew R and Buchanan M 2004 Optimized GaAs/AlGaAs light-emitting diodes and high efficiency wafer-fused optical up-conversion devices *J. Appl. Phys.* **96** 5243

[13] Dupont E, Gao M, Buchanan M, Wasilewski Z R and Liu H C 2001 Optimization of p-doping in GaAs photon-recycling light-emitting diodes operated at low temperature *Semicond. Sci. Technol.* **16** 21

[14] Liu H C, Allard L B, Buchanan M and Wasilewski Z R 1997 Pixelless infrared imaging device *Electron. Lett.* **33** 5

[15] Sadi T, Radevici I, Kivisaari P and Oksanen J 2019 Electroluminescent cooling in III–V intracavity diodes: practical requirements *IEEE Trans. Electron Devices* **66** 2

[16] Sadi T, Kivisaari P, Tiira J, Radevici I, Haggren T and Oksanen J 2018 Electroluminescent cooling in intracavity light emitters: modeling and experiments *Opt. Quantum Electron.* **50** 18

[17] Incandela R M, Song L, Homulle H, Charbon E, Vladimirescu A and Sebastiano F 2018 Characterization and compact modeling of nanometer CMOS transistors at deep-cryogenic temperatures *IEEE J. Electron. Devices Soc.* **6** 996

[18] Charbon E, Sebastiano F, Vladimirescu A, Homulle H, Visser S, Song L and Incandela R M 2016 Cryo-CMOS for quantum computing *2016 IEEE International Electron Devices Meeting (IEDM)* 5, 13

[19] Imangholi B, Hasselbeck M P, Bahae M S, Epstein R I and Kurtz S 2005 Effects of epitaxial lift-off on interface recombination and laser cooling in GaInP/GaAs heterostructures *Appl. Phys. Lett.* **86** 081104

[20] Schubert E F 2006 *Light-Emitting Diodes.* (Cambridge: Cambridge University Press) (https://doi.org/10.1017/cbo9780511790546)

[21] Zhang S, Wang T M, Hao M R, Yang Y, Zhang Y H, Shen W Z and Liu H C 2013 Terahertz quantum-well photodetectors: design, performance, and improvements *J. Appl. Phys.* **114** 194507

[22] Bai P *et al* 2019 Broadband THz to NIR up-converter for photontype THz imaging *Nat. Commun.* **10** 1–9

[23] Neamen D A 2012 *Semiconductor Physics and Devices: Basic Principles.* (New York: McGraw-Hill)

[24] Vening M, Dunstan D J and Homewood K P 1993 Kxciton dynamics in InGaAs/GaAs quantum-well heterostructures: competition between capture and thermal emission *Phys. Rev.* B **48** 2412

[25] Cho J, Schubert E F and Kim J K 2013 Efficiency droop in light-emitting diodes: challenges and countermeasures *Laser Photon. Rev.* **7** 408

[26] Karpov S 2015 ABC-model for interpretation of internal quantum efficiency and its droop in III-nitride LEDs: a review *Opt. Quantum Electron.* **47** 1293

[27] Piprek J 2010 Efficiency droop in nitride-based light-emitting diodes *Phys. Status Solidi* A **207** 2217

[28] Ryu H, Kim H and Shim J 2009 Rate equation analysis of efficiency droop in InGaN light-emitting diodes *Appl. Phys. Lett.* **95** 081114

[29] Wasilewski Z R, Dupont E, Weyher J L, Laframboise S, Buchanan M and Liu H C 2010 On the existence of submicron diameter current shunts in morphologically perfect device layers *J. Cryst. Growth* **312** 926

[30] Bai P, Zhang Y H, Guo X G, Fu Z L, Cao J C and Shen W Z 2018 Realization of the high-performance THz GaAs homojunction detector below the frequency of Reststrahlen band *Appl. Phys. Lett.* **113** 241102